PROTEINS: Structure, Function, and Genetics 5:183–201 (1989)

The Crystal Structure of the Ternary Complex of Staphylococcal Nuclease, Ca^{2+}, and the Inhibitor pdTp, Refined at 1.65 Å

Patrick J. Loll and Eaton E. Lattman
Department of Biophysics, The Johns Hopkins University School of Medicine, Baltimore, MD 21205

ABSTRACT **The structure of a complex of staphylococcal nuclease with Ca^{2+} and deoxythymidine 3′,5′-bisphosphate (pdTp) has been refined by stereochemically restrained least-squares minimization to a crystallographic *R* value of 0.161 at 1.65 Å resolution. The estimated root-mean-square (rms) error in the coordinates is 0.16 Å. The final model comprises 1082 protein atoms, one calcium ion, the pdTp molecule, and 82 solvent water molecules; it displays an rms deviation from ideality of 0.017 Å for bond distances and 1.8° for bond angles.**

The mean distance between corresponding α carbons in the refined and unrefined structures is 0.6 Å; we observe small but significant differences between the refined and unrefined models in the turn between residues 27 and 30, the loop between residues 44 and 50, the first helix, and the extended strand between residues 112 and 117 which forms part of the active site binding pocket.

The details of the calcium liganding and solvent structure in the active site are clearly shown in the final electron density map. The structure of the catalytic site is consistent with the mechanism that has been proposed for this enzyme. However, we note that two lysines from a symmetry-related molecule in the crystal lattice may play an important role in determining the geometry of inhibitor binding, and that only one of the two required calcium ions is observed in the crystal structure; thus, caution is advised in extrapolating from the structure of the complex of enzyme and inhibitor to that of enzyme and substrate.

Key words: crystallographic refinement, restrained least-squares refinement, Konnert–Hendrickson refinement, phosphodiesterase, protein structure, enzyme mechanism

INTRODUCTION

Staphylococcal nuclease (nuclease) has been used for many years as a model protein in studies of protein folding and enzymatic catalysis.[1–4] It contains only 149 residues, carries no disulfide bonds or free sulfhydryl groups, and can be unfolded and refolded reversibly. The protein is originally derived from the bacterium *Staphylococcus aureus,* but the gene for nuclease has been cloned[5] and inserted into several expression systems.[6,7] A large number of mutant forms of nuclease have been generated by both random[6] and site-directed mutagenesis,[8] and are rich sources of biochemical and biophysical data relating to the structural and functional consequences of altering the protein's amino acid sequence. We have undertaken a study of the three-dimensional structures of several mutant forms of nuclease in an attempt to understand at the atomic level the effects of altering the protein's primary structure.

The structure of the complex of nuclease, pdTp, and Ca^{2+} was determined in the laboratories of Cotton and Hazen.[9] In order to have the most accurate possible benchmark structure against which to compare our mutant structures, we have refined the structure of the ternary complex of wild-type nuclease with pdTp and Ca^{2+} using a stereochemically restrained, least-squares minimization method. We report here this highly refined structure at a resolution of approximately 1.65 Å.

MATERIALS AND METHODS

Crystallization

Wild-type nuclease is expressed by an engineered strain of *E. coli* carrying the plasmid pFOG405. The initial protein purification was carried out essentially as described,[10] yielding 95–99% pure nuclease; after this procedure, instead of being lyophilized, the protein was dialyzed against 25 mM potassium phosphate, pH 7.6, and then loaded onto an hydroxyapatite column (Bio-Rad: BioGel HTP) equilibrated with the same buffer. The column was washed with several column volumes of buffer, after which nuclease was eluted with a linear gradient

Received December 29, 1988; accepted February 17, 1989.

Address reprint requests to Patrick J. Loll, Department of Biophysics, Johns Hopkins University School of Medicine, 725 N. Wolfe St., Baltimore, MD 21205.

from 25 mM potassium phosphate to 500 mM potassium phosphate, pH 7.6. Fractions corresponding to the nuclease peak were pooled, dialyzed against 10.5 mM potassium phosphate, pH 8.15, and concentrated to a final concentration of 25–30 mg ml^{-1}. Purified, concentrated protein was stored at 4°C for 1 month with no apparent proteolysis or loss in activity.

Crystals of the complex of nuclease with Ca^{2+} and pdTp were grown by a modification of the published method.[11,12] MPD (Aldrich, Gold Label) was added slowly, with mixing, to a 20 mg ml^{-1} solution of protein in 10.5 mM potassium phosphate, pH 8.15, to a final concentration of 17% (weight-to-weight). This solution was allowed to sit at 4°C for approximately 60 hours. At this point, 1.1 molar equivalents of pdTp (as a 2 mg ml^{-1} solution in water) and 2 molar equivalents of Ca^{2+} (as a 10 mM $CaCl_2$, 20 mM potassium citrate solution) were added to the protein solution and the mixture was filtered through a 0.45-μm filter. Vapor diffusion crystallization trays[13] were then set up as follows: Drops of the filtered solution were placed on siliconized cover slips, which were inverted over wells containing solutions of MPD in 10.5 mM potassium phosphate, ranging from 21 to 23% MPD (w/w). Trays were kept at 4°C; crystals appeared in 2–3 weeks, and grew rapidly to a size of 0.5 × 0.5 × 1.0 mm.

The complex of wild-type nuclease with Ca^{2+} and pdTp crystallizes in the space group $P4_1$, with $a = b = 48.0$ Å and $c = 63.5$ Å.

Data Collection

Room temperature X-ray diffraction data were collected from three different crystals at the Multiwire Area Detector facility at the University of North Carolina. The data were scaled and merged using the program FS (L. Weissman, C. Stauffacher, and D. Eisenberg, unpublished program). Although this program has the capability of fitting a correction surface, modeled by a low order two-dimensional Fourier series, to each virtual film in the data set, we did not employ this option, and scaled together all films with flat unitary correction surfaces; 49,178 intensity measurements were made of 11,645 independent reflections. After scaling and Lorentz and polarization corrections, reflections having mean intensities less than three times the standard deviation of the intensity ($I/\sigma<3$) were rejected. We were left with a data set comprising 11,332 reflections lying in the resolution range 10–1.6 Å, exhibiting a merging R value on intensities (R_{symm}) of 0.022. The overall R_{symm} was equal to 0.025 prior to outlier rejection, and thus was improved hardly at all. The values for R_{symm} in the high-resolution ranges improved drastically after outlier rejection, however; e.g., outlier rejection caused R_{symm} in the resolution range 1.7–1.65 Å to go from 0.38 to 0.19. The dependence of R_{symm} on resolution is shown in Figure 1. The final data set is 61% complete in the range 10–1.6 Å. It is 85% complete in the range 10–1.9 Å; in the high-resolution shell 1.7–1.6 Å, it is only 30% complete.

When evaluating a data set, it is useful to calculate the parameter D2 proposed by Howard (A. Howard, personal communication); this parameter is calculated as follows. The data set is divided up into thin shells of differing resolutions. For each reflection in a given shell, the ratio of the reflection's intensity to its estimated standard deviation is calculated. The mean of this ratio for all reflections in a given shell is then computed. D2 is defined as the resolution at which this mean ratio of I/σ falls below 2. D2 gives the investigator an objective measure of the effective resolution of a data set. We have calculated D2 for this data set to be 1.66 Å. It should be noted that after scaling our data, we discarded all reflections having I/σ less than 3. Thus, while the D2 calculation yields an idea of the manner in which the quality of the diffraction data deteriorates with increasing resolution, its precise significance for the subset of the data against which we have refined the model is not obvious.

Refinement

Structure refinement was performed using the stereochemically restrained least-squares program PROLSQ of Hendrickson and Konnert.[14] Our version of PROLSQ has been modified to accommodate symmetry-related contacts within the crystal[15] and to allow for discretely disordered side chains.[16]

As a starting model for the refinement, we used the 1.5 Å wild-type/Ca^{2+}/pdTp complex structure from the laboratories of Cotton and Hazen[9] which has been deposited in the Brookhaven Protein Data Bank.[17,18] Structure factors calculated from this model, assuming an overall temperature factor (i.e., Debye–Waller factor) of 15 $Å^2$, yielded a crystallographic residual of 0.45 over the resolution range 20–1.6 Å.

The program PROLSQ restrains the geometry of the molecule(s) being refined so as to minimize the difference between the model's geometry and "ideal" geometry. The "ideals file" supplied with the program contains information about ideal protein geometry, but, obviously, has no information about the

Abbreviations: MPD, 2-methyl-2,4-pentanediol; pdTp, deoxythymidine 3',5'-bisphosphate; R_{symm}, symmetry R value on intensities defined as follows:

$$R_{symm} = \frac{\sum_{\mathbf{h}}\sum_{j} | I(\mathbf{h})_j - \bar{I}(\mathbf{h}) |}{\sum_{\mathbf{h}}\sum_{j} I(\mathbf{h})_j}$$

where $I(\mathbf{h})_j$ represents the jth observation of the intensity at reflection $\mathbf{h}$.

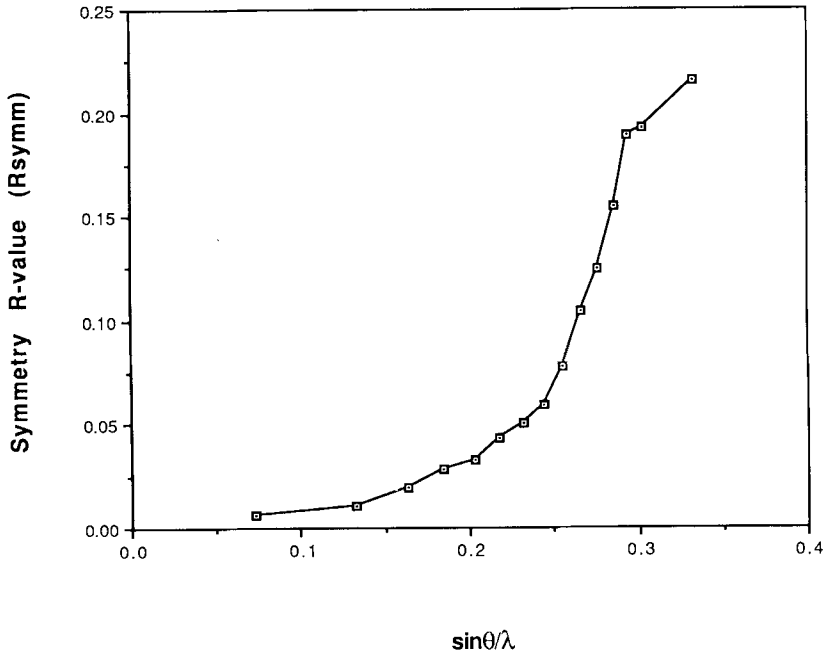

Fig. 1. Dependence of the symmetry R value R_{symm} on resolution. These values represent R_{symm} calculated for shells of resolution, using the final, reduced data set of 10,497 unique reflections with more than one observation having $I/\sigma>3$.

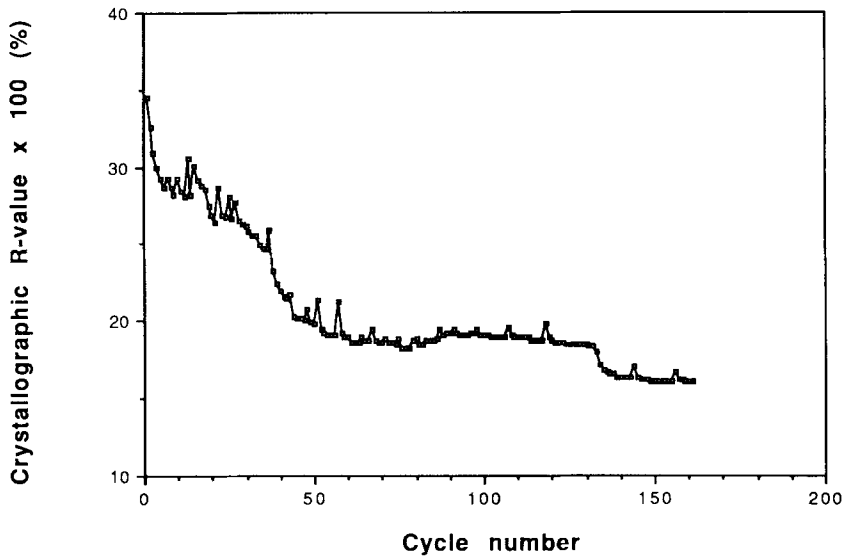

Fig. 2. Course of the refinement. Note the large drops in the residual after cycle 36, when the program CONNEX was repaired so that the scattering of the inhibitor pdTp could be properly accounted for, and after cycle 132, when an overall anisotropic ΔB was included in the model.

mononucleotide inhibitor pdTp present in our crystals. Accordingly, we inserted this information into the ideals file using the program CONNEX, kindly supplied by Dr. Arno Pahler. The model we used to generate the paradigm for the pdTp structure was derived from the crystal structure of a B-form DNA dodecamer[19] found in the Protein Data Bank.

Throughout the refinement, the following strategy was employed: Successive cycles of PROLSQ were run until convergence was obtained. At this point, difference Fourier maps were calculated and inspected; the model was changed as necessary and then placed back into PROLSQ. Several types of difference Fourier maps were used: $2F_o-F_c$, ϕ_c maps (phases ϕ_c calculated from the model), F_o-F_c, ϕ_c maps (phases again calculated from the model; these

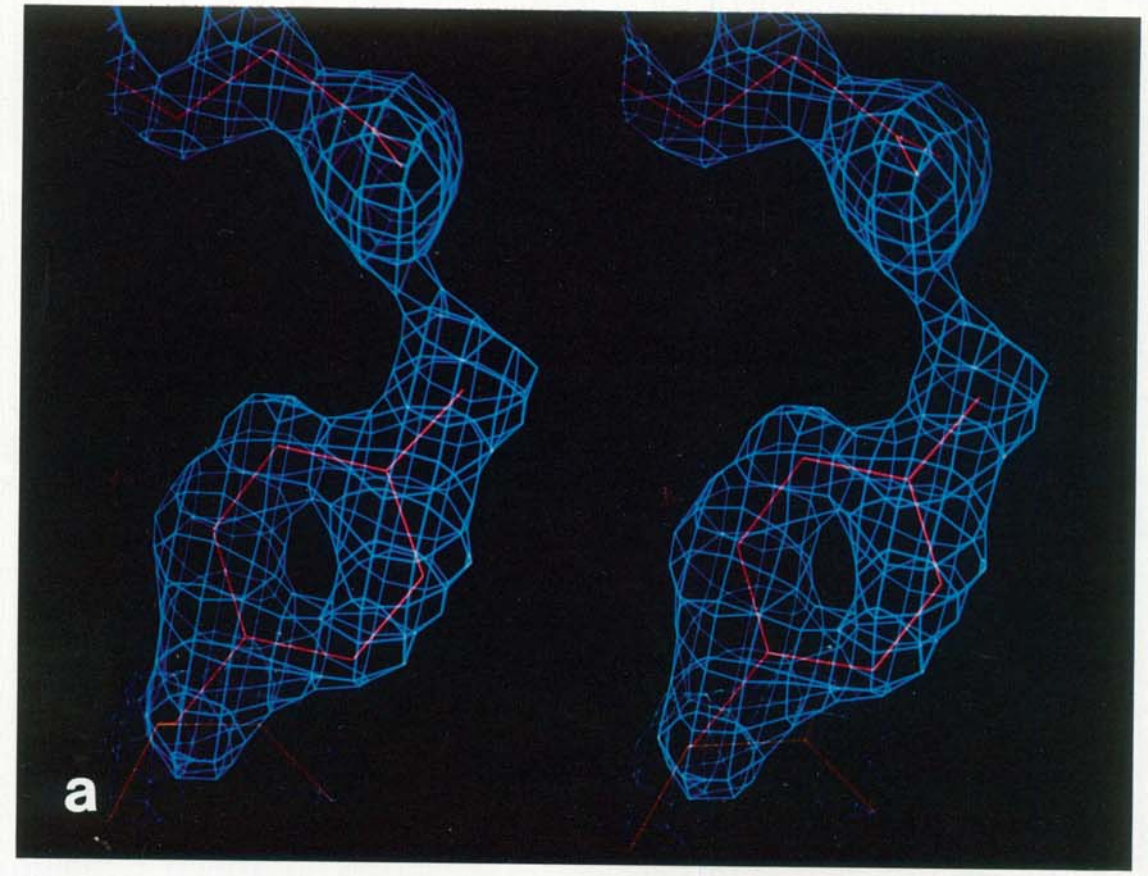
a

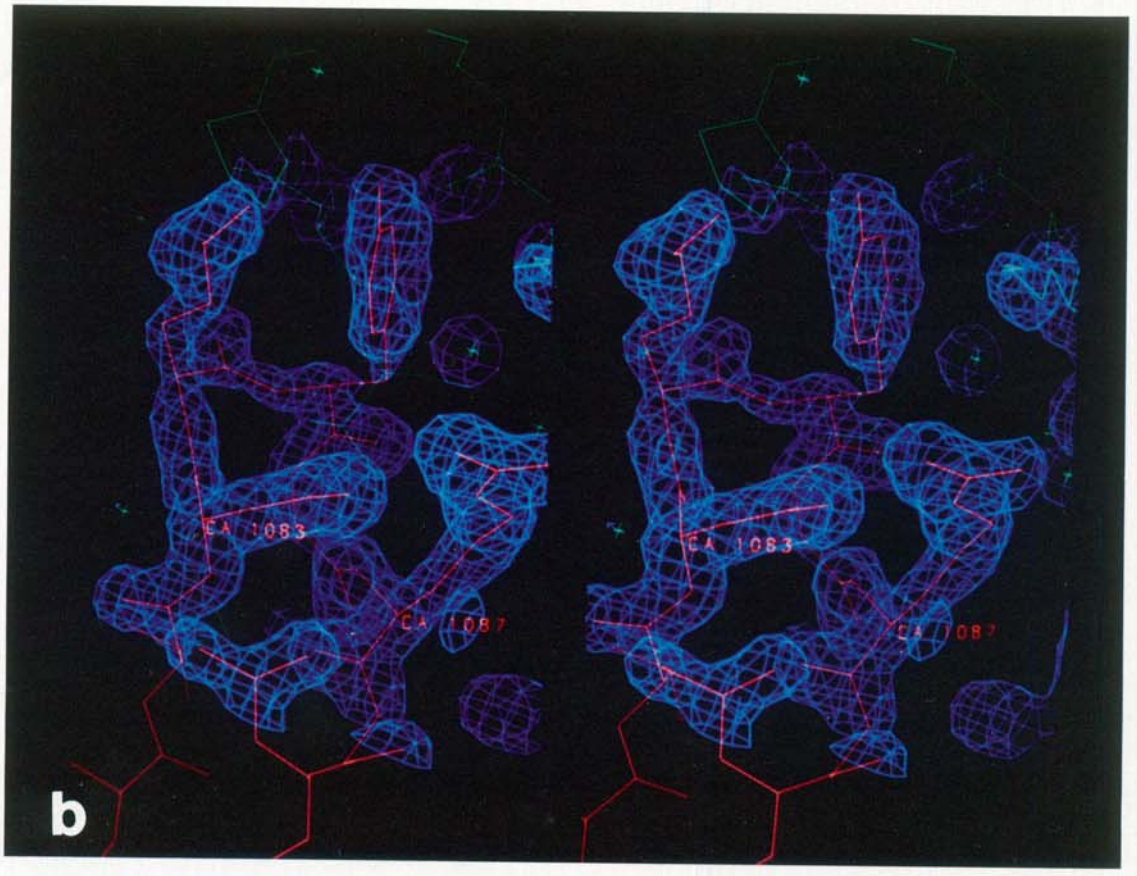
CA 1083
CA 1087
CA 1083
CA 1087
b

are also referred to as ΔF maps), and residue delete maps, which are similar to the $2F_o-F_c$, ϕ_c maps, except that the model from which the structure factor calculation is made is missing anywhere from 1 to 10 residues. This last synthesis is useful for eliminating model bias from the electron density map. In general, the $2F_o-F_c$ maps (both the normal and residue delete maps) were most useful in the early and middle stages of the refinement, when relatively gross changes were being made to the model. The ΔF maps became most useful in the final stage of refinement, when solvent atoms were being added to the model and relatively small changes were being made in side chain configurations. The maps were examined and the model was manipulated using the program FRODO[20] on the Evans and Sutherland PS300 picture system. All through the refinement, we relied heavily on W. Steigemann's PROTEIN system of crystallographic software.[21]

The course of the refinement is illustrated in Figure 2. We began by refining against data in the resolution range 10–3 Å. After cycle 12, we started to expand the set of observed structure factors used in the refinement in a stepwise manner, including more and more high-resolution data and removing data at very low resolution (since inadequate modeling of the disordered solvent gives rise to large discrepancies between observed and calculated structure factors at very low resolution). By cycle 30, we were refining against data in the range 6–1.6 Å. This resolution range was not changed for the remainder of the refinement. For the first 17 cycles, only positional shifts were applied to the model; after cycle 17, shifts in individual atomic temperature factors were applied as well.

The weight applied to the structure factor term in the refinement of a protein structure is typically a function of the mean difference between observed and calculated structure factor amplitudes, $\langle||\mathbf{F}_o| - |\mathbf{F}_c||\rangle$ (for brevity, we will henceforth write this quantity as $\langle F_o-F_c\rangle$). PROLSQ calculates the dependence of $\langle F_o-F_c\rangle$ on resolution, fitting the linear relation

$$\langle F_o-F_c\rangle_{\sin(\theta/\lambda)} = a' + b'(\sin\theta/\lambda)$$

to the data. For the first 32 cycles of refinement, we weighted the structure factor term with a weight of the form

$$\text{weight} = 1/\sigma^2$$

where

$$\sigma = a + b(\sin\theta/\lambda)$$

and

$$a = a'/2$$
$$b = b'/2$$

The effect of using this form for the structure factor weight is to make the crystallographic residual approximately equal in all shells of resolution. This is useful when one is adding in high-resolution data; the resolution-dependent σ allows one to rapidly bring down the residual for the newly added data to a level comparable to the other data's residual. After cycle 32, however, we changed to a single σ given by $\sigma = 1/2\langle F_o-F_c\rangle$, where $\langle F_o-F_c\rangle$ represents a single value calculated over the entire data set. This allowed the residual to revert to low values at low resolution, where the structure factors are large and well measured, and high values at high resolution, where the structure factors are weak and the agreement statistics are correspondingly worse (see Fig. 1).

After cycle 36, it was noticed that the residual R values calculated in PROLSQ did not agree with those calculated in the PROTEIN system. We then discovered that the geometric restraint information for the pdTp molecule had not been properly inserted into the ideal geometry file by the program CONNEX. As a result, PROLSQ was ignoring the inhibitor and was calculating structure factors from a model consisting of the protein atoms only. We corrected this, and the overall R value dropped rapidly in the subsequent cycles.

We began to incorporate solvent atoms into the model after cycle 36. We used two criteria to determine whether or not a water molecule should be placed in a region of density: (1) The density should look approximately spherical and be seen in the ΔF map as well as the $2F_o-F_c$ map, and (2) the fitted water should be within a reasonable hydrogen bonding distance from some proton donor or acceptor (no account was taken of the hydrogen bond geometry at this stage). As the refinement progressed, we continued to place water molecules in the model as they became visible. After cycle 127 we began to refine occupancies for the solvent molecules; occupancy shifts and temperature factor shifts were applied in alternate cycles. Waters were deleted from the model if their occupancies refined to a value below 0.5 or if their temperature factors refined to a value above 60 Å^2.

After cycle 132, we included in the model an anisotropic overall ΔB, calculated using the program

Fig. 3. Stereo views of two regions of the final electron density map with the refined model superimposed. In both panels the map is an OMITMAP (see ref. 32) contoured at 2.5 standard deviations. **a:** The hydrogen bond between Asp-10 and Tyr-27. **b:** The reverse turn spanning residues 83 through 87. The sequence of this 5-residue section is as follows: Asp-Lys-Tyr-Gly-Arg. The green residues at the top of the figure are part of an adjacent molecule in the crystal lattice. Note that the residue numbers in the figure have one thousand added to them, i.e., residue 83 is labeled as 1083, etc..

ANISOB supplied by Dr. Steven Sheriff.[22] Since nuclease crystallizes in a tetragonal space group, we constrained the off-diagonal terms of the anisotropic ΔB tensor (i.e., b_{12}, b_{13}, and b_{23}) to be zero. The residual immediately dropped from 0.184 to 0.169; in addition, the standard deviation of the ΔF electron density map was reduced by >10% (from 0.058 electrons/Å^3 to 0.052 electrons/Å^3) and a number of troublesome peaks in the ΔF map whose existence could not be ascribed to model error disappeared. The precise significance of the observed anisotropy is not clear; we have no way of knowing if it derives from genuine anisotropy of thermal motion, anisotropic disorder, or systematic errors in the data. However, given a caveat against overinterpretation of the physical significance of the overall ΔB, we feel that the inclusion of an additional three parameters in the model is well justified by the improvements it brings to the residual and the maps. The components of the anisotropic ΔB tensor were recalculated every few cycles; the values associated with the final refined model were calculated to be $b_{11} = 5.3 \pm 0.16$ Å^2, $b_{22} = 5.1 \pm 0.16$ Å^2, and $b_{33} = -2.5 \pm 0.13$ Å^2. b_{11} and b_{22} are expected to be equal for a tetragonal space group; the fact that they refined to the same value (± 1 standard deviation), without being constrained to be equal gives us further confidence in the quality of the data. In order to facilitate the comparison of this structure with other structures which may not include overall anisotropic thermal parameters, we adjusted the overall anisotropic ΔB so that the trace equals zero, i.e., $b_{11} + b_{22} + b_{33} = 0$. To compensate, we added 2.6 Å^2 to the individual isotropic temperature factor of each atom.

The parameter shifts calculated in each cycle of PROLSQ are only estimates; we employed a feature of the program that evaluates the impact of these shifts on the R value after each cycle, which allowed us to gauge an appropriate shift damping factor to be applied to each shift for each cycle. It is noteworthy that the optimal shift damping factors were almost never the same for two successive cycles; in fact, attempts to automate the process by running large batch jobs containing many cycles with the same shift damping factors applied after each cycle usually led to stagnant or increased R values.

Tables I and II summarize the refinement parameters as they stand at the end of the refinement. The geometry of the model is quite good. We have not found it necessary to invoke the presence of multiple side chain conformations for any residue to explain the observed density. While we have no doubt that populations of different conformers exist for many, if not most side chains,[16] it appears that they cannot be resolved into some small number of discrete conformers in this structure. It is to be expected that certain of the surface side chains which are not involved in crystal contacts will be disordered in any protein crystal structure. In our case, we expect more than the average number of disordered side chains, as staphylococcal nuclease is extremely basic (pI = 9.6) and 21 of the 135 residues we can see in our electron density maps are lysines, which tend to be flexible and located at the molecular surface. A list of the side chains for which we see poor or no density is as follows: His-8, Lys-28, Gln-30, Lys-45, His-46, Lys-48, Lys-49, Lys-53, Lys-97, Lys-133, and Lys-134.

The final ΔF map has a standard deviation of 0.048 electrons/Å^3, and contains no peaks greater than 0.24 electrons/Å^3, and only two peaks greater than 0.22 electrons/Å^3—one is near the side chain of Gln-80, which is a slightly disordered side chain, and the other is near the α carbon of Gly-20, for which we can offer no explanation. There are only two negative peaks lower than −0.22 electrons/Å^3; one is centered on the side chain of His-8 (−0.26 electrons/Å^3), which we believe is disordered in the crystal structure, and the other is near the backbone at Asp-77 (−0.24 electrons/Å^3), which we cannot explain. The quality of the final electron density maps may be seen in Fig. 3.

RESULTS AND DISCUSSION

Quality of the Model

There exists no rigorous method to calculate the coordinate errors associated with a structure refined by restrained least-squares methods. There are, however, several approximate calculations which one may use to obtain a rough idea of the errors in a given structure. One such calculation is that derived by Cruickshank,[23–25] which attempts to estimate the standard deviation of positions from the standard deviation of the electron density. Performing this calculation for the refined nuclease model leads to an estimated rms coordinate error of 0.16 Å. Cruickshank's derivation gives an expression for the error in any atomic coordinate that, for a given structure, is a function of the atom's type (carbon, nitrogen, etc.) and temperature factor only. Thus, we can estimate the standard deviation of the position of each atom in the structure. A histogram of these calculated standard deviations is shown in Figure 4a; Figure 4b shows the dependence of the calculated standard deviations on temperature factor for the different atom types present in the structure.

Another, independent method for estimation of coordinate error is that of Luzzati.[26] This method assumes that the only error present is coordinate error. Plotting the crystallographic residual versus resolution enables one to estimate the mean coordinate error for the structure. From such a plot (shown in Fig. 5) we obtain an estimate of approximately 0.15–0.18 Å, in close agreement with the Cruickshank method.

Yet a third estimate of errors in the structure was obtained as follows: The refined wild-type structure

TABLE I. Crystallographic Parameters at the End of Refinement

R value	0.161
$\langle F_o - F_c \rangle$	19.4
Final σ*	9.6
Resolution range	6.0–1.6 Å
No. of reflections	11,332
No. of atoms	1190
No. of water molecules	82
Mean B (Å^2)	26.6
No. of cycles elapsed	172
Rms coordinate shift calculated in final cycle	0.01 Å

*Weight applied to structure factor term in refinement is $1/\sigma^2$.

TABLE II. Final Weighting Parameters and Deviations from Ideal Geometry

Restraint	rms deviation	Target σ*
Distances (Å)		
Bond distances	0.017	0.015
Angle distances	0.037	0.025
Planar 1–4 distances	0.050	0.040
Planar groups (Å)	0.020	0.017
Chiral volumes (Å^3)	0.157	0.150
Torsional angles (degrees)		
Planar	3.2	3.0
Staggered	22.0	15.0
Orthonormal	25.6	20.0
Thermal factors (Å^2)		
Main chain bond	1.07	1.00
Main chain angle	1.82	1.50
Side chain bond	1.47	1.00
Side chain angle	1.52	1.50

*Weights applied to restraint terms in the refinement are of the form weight = 1/(target σ)^2.

was superimposed on the refined structure of the Glu-43→Asp mutant of nuclease complexed with pdTp and Ca^{2+} (P. J. Loll, and E. E. Lattman, unpublished results), and the rms difference in C_α positions was calculated to be 0.18 Å. We argue that this suggests that the error in the wild-type coordinates is less than 0.16 Å, and offer two reasons. (1) Real differences exist between the two structures. (2) Suppose the E43D structure is identical to that of the wild type; then the coordinate difference would be due to random coordinate errors. In this case, if the coordinate error is *identical* for both structures, the observed difference in C_α positions is consistent with this coordinate error being 0.13 Å [coordinate difference $\Delta r = (\sigma^2_{\text{wild type}} + \sigma^2_{\text{E43D}})^{1/2}$]; however, the E43D structure has a higher R value (0.186),and is refined at a slightly lower resolution (approximately 1.8 Å), and thus its coordinate errors are expected to predominate over those of the wild type in a comparison of this sort.[27] Thus, this crude analysis suggests that 0.16 Å is a conservative estimate of the mean coordinate error in the refined wild-type structure.

Polypeptide Conformation

The overall conformation of the polypeptide chain is similar to that observed in the earlier structure[9]; the locations of different elements of secondary structure are summarized in Table III, and a stereo view of the folding of the polypeptide chain can be seen in Figure 6. A description of the intramolecular hydrogen bonding pairs we have observed (exclusive of those involving solvent atoms or the pdTp molecule) is presented in the Appendix.

The first amino acid for which we observe electron density is Leu-7. From residue 7, an elongated region leads into the first four strands of antiparallel β sheet. After exiting from the third strand, the chain alters its direction, and with this turning point forms the floor of the active site in the region of residues 36–40. The chain continues into a large loop comprising residues 44–50 which we find to be somewhat disordered and/or mobile. We observe weak, but interpretable density for the backbone throughout this stretch. After the loop, the chain enters the first helix, spanning residues 54–68. This is followed by two antiparallel β strands, separated by a loop (residues 77–87), which forms the top of the active site. The two β strands, together with the four strands mentioned earlier, make up a Greek key antiparallel β barrel.[28] These strands are followed by helix 2, which comprises residues 98 to 106. Helix 2 ends in one turn of 3_{10} helix, followed by one residue (Gly-107) in the left-handed α conformation. This type of conformation has been observed frequently at the C-termini of helices,[30] and allows for a 1→6 hydrogen bond between the carbonyl oxygen of residue 103 and the amide nitrogen of residue 108. Helix 2 is followed by an extended segment, which terminates in the type VIa turn between residues 115 and 118 that contains the *cis*-proline 117. The third helix runs from residue 121 to residue 135, and ends in the same α_L conformation as does helix 2; in fact, the peptide backbone between residues 131 and 137 is virtually superimposable on the stretch of backbone running from residue 102 to 108. Helix 3 is followed by a turn containing the protein's sole tryptophan, residue 140. We can observe no density for any residue after Ser-141, and conclude that the C-terminus, like the N-terminus, is disordered.

We count a total of 10 reverse turns in the protein. The placement of two turns back-to-back in residues 155–122 is noteworthy; it is interesting that the second of these two turns, the type I turn spanning residues 119–122, serves to provide a hydrogen bond acceptor for the amide proton of residue 122, an early residue in helix 3. Helix 2 starts off in a similar fashion, being preceded by a type II turn comprising residues 52–55. Presta and Rose recently pointed out the importance of providing hydrogen bond acceptors to stabilize the N-termini of helices,[30] but concentrated on the role of side chains in this hydrogen bonding; it appears that a reverse turn imme-

TABLE III. Summary of Secondary Structure

Helices		Residue range
1		54–68
2		98–106
3		121–135
Antiparallel strands*		
1		7–10
2		13–19
3		21–27
4		29–35
5		71–83
6		91–95
Reverse turns	Residue range	Turn type†
1	19–22	I
2	27–30	I′
3	46–49	I
4	52–55	II
5	83–86	I
6	94–97	I′
7	115–118	VIa
8	119–122	I
9	137–140	II′
10	138–141	I

*We observe two β bulges[28]: one involving residues 15, 16, and 24 and the other involving residues 18, 19, and 22.
†See ref. 28.

diately before the helix can also help satisfy this requirement.

The backbone torsion angles φ and ψ of the refined structure are displayed in a Ramachandran diagram in Figure 7. All nonglycine residues of the protein are shown to fall into favorable regions of the energy surface, with the exception of Asn-138, which is in position 2 of a type II′ turn, a sterically unfavored configuration. However, deletion of the residue from the model, followed by refinement (to remove residual bias) and calculation of an electron density map, convincingly showed that the turn as modeled is correct (data not shown). Evidently, the interactions allowed by this conformation are sufficiently favorable that they offset the unfavorable steric contribution associated with this φ, ψ position (for example, the side chain of Asn-138 is seen to hydrogen bond to the carbonyl oxygen of residue 106, perhaps helping to "tack down" helix 3 onto the main body of the protein).

A histogram showing the distribution of the χ^1 torsion angles for all the side chains in the structure is shown in Figure 8. As noted by Janin et al.,[31] the angles are clustered into three groupings at approximately ± 60°, 180°, in accordance with predictions based on simple energy considerations. One must be cautious in interpreting these angle distributions, however, as most refinement programs, including PROLSQ, include energy or stereochemistry terms which tend to drive torsional angles toward ideal values. Such a term was used in this refinement, and, although we weighted it weakly, it still may have had some prejudicial effect on the outcome. On the other hand, at the resolution at which we are working, the conformation of any ordered side chain can be unambiguously derived from the electron density, and thus any errors in side chain torsional angles should be evident in residue delete maps or OMITMAPS.[32] We do not see evidence for any such errors.

Comparison of the Refined and Unrefined Models

As noted above, no drastic modifications were made in the model during the course of the refinement. Many small differences exist, however; after superposition of the refined and unrefined structures using a least-squares method to minimize C_α–C_α distances, we calculated the rms C_α–C_α distance to be 0.6 Å. A plot of these C_α–C_α distances versus residue number is shown in Figure 9. As can be seen, the refined model deviates significantly from the earlier model in several places. For example, the turn type of the turn between residues 27–30 has been changed from type IV to type I′. The flexible loop region (residues 43–50) has changed a great deal. Helix 1 is considerably more uniform in the refined model than in the unrefined model. In the unrefined model, the helix displays a mixture of normal α helix and 3_{10} helix hydrogen bonding, whereas the helix in the refined model is all α helical, with all the possible 1→4 hydrogen bonds from residues 55 through 64 being made. The protein backbone immediately following helix 1, at residues 70–72, has changed markedly during the refinement, moving as much as 1.5 Å. However, the side-chains of residues 70 and 71, which protrude into the active site of an adjacent protein molecule in the crystal lattice, did not move very far during the refinement. Perhaps the largest changes between the refined and unrefined structures are to be found in the extended region spanning residues 113–117. Both backbone and side chain conformations have been altered markedly in the refinement. Of particular interest are the side chains of tyrosines 113 and 115, which are seen to interact with the inhibitor pdTp. In the refinement, the tyrosine ring of residue 113 has moved closer to the sugar of the pdTp, packing against it. The phenolic ring of tyrosine 115, the plane of which was modeled to be parallel to that of the inhibitor's pyrimidine ring, is now seen to be almost perpendicular to the pyrimidine.

Structure of the Active Site; Implications for the Mechanism

A schematic diagram of the active site is shown in Figure 10; a detailed picture of the model in the same region is shown in Figure 11. We confirm many of the features of the active site geometry noted by Cotton et al.[9] and are able to contribute additional structural details to the analysis.

The inhibitor pdTp fits into a cleft, with the aro-

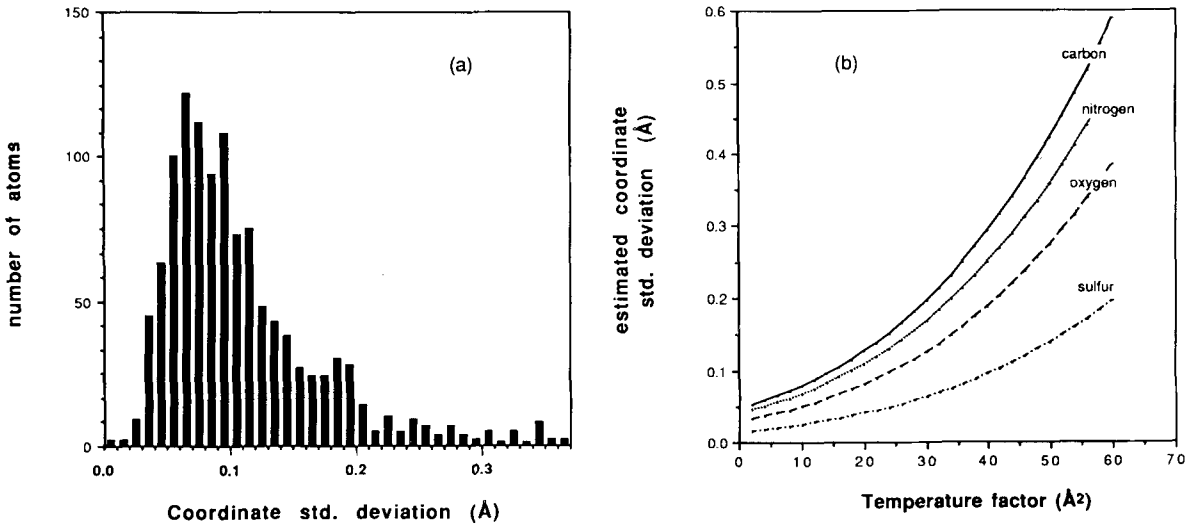

Fig. 4. **a:** Distribution of atomic coordinate standard deviations as estimated by Cruickshank's method. **b:** Dependence of atomic coordinate standard deviation upon individual atomic temperature factor illustrated for four different atom types.

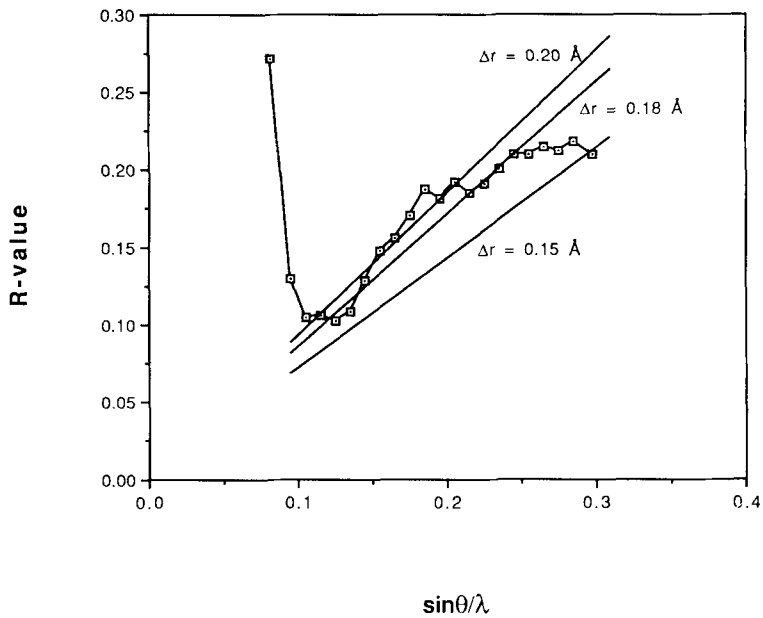

Fig. 5. Luzzati plot for refined structure. Superimposed upon the data are theoretical curves derived for three values of the coordinate error Δr.

matic ring in a hydrophobic pocket at the base of the cleft. The nucleotide base makes no specific contacts with the enzyme; its N3 and O4 atoms are seen, rather, to hydrogen bond to a string of water molecules occupying the top of the active site. The 3′- and 5′-phosphates are firmly anchored by a number of hydrogen bonds and ionic interactions.

The 3′-phosphate is the more exposed of the two phosphate groups; it is seen to hydrogen bond to the side chains of Lys-84 and Tyr-85, but it is at the top of the cleft, and is still largely accessible to solvent. The 5′-phosphate, on the other hand, is almost completely buried, and, while inaccessible to bulk solvent, is involved in a large number of favorable interactions with groups on the protein. (It is the 5′-phosphate which is thought to occupy a position close to that occupied by the scissile phosphoester link in the productive complex of enzyme with calcium ion and substrate.) Two of its oxygens are involved in a double hydrogen bond with the ϵ nitrogen and one of the terminal amines of Arg-35, in a bonding pattern reminiscent of the type 1 arginine-

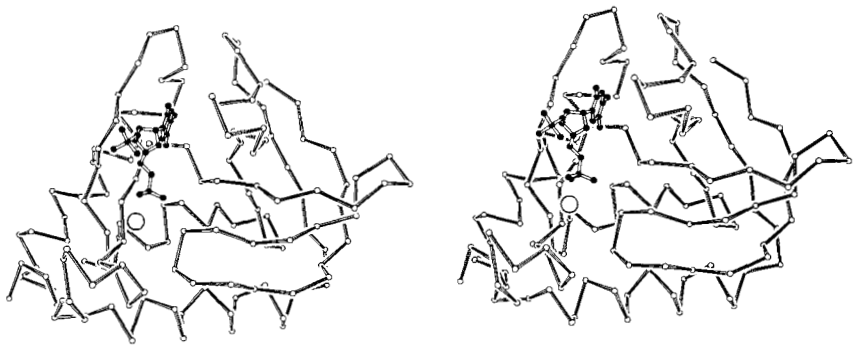

Fig. 6. Stereo drawing of the C_α backbone of the refined structure. The protein backbone is drawn with dark bonds and light atoms; the inhibitor pdTp is drawn with light bonds and dark atoms. Also shown is the calcium ion, depicted as a large sphere immediately below the pdTp molecule. The protein's N-terminus appears at the upper right in this view; the C-terminus is at the lower left. This drawing was made using the program ORTEP.

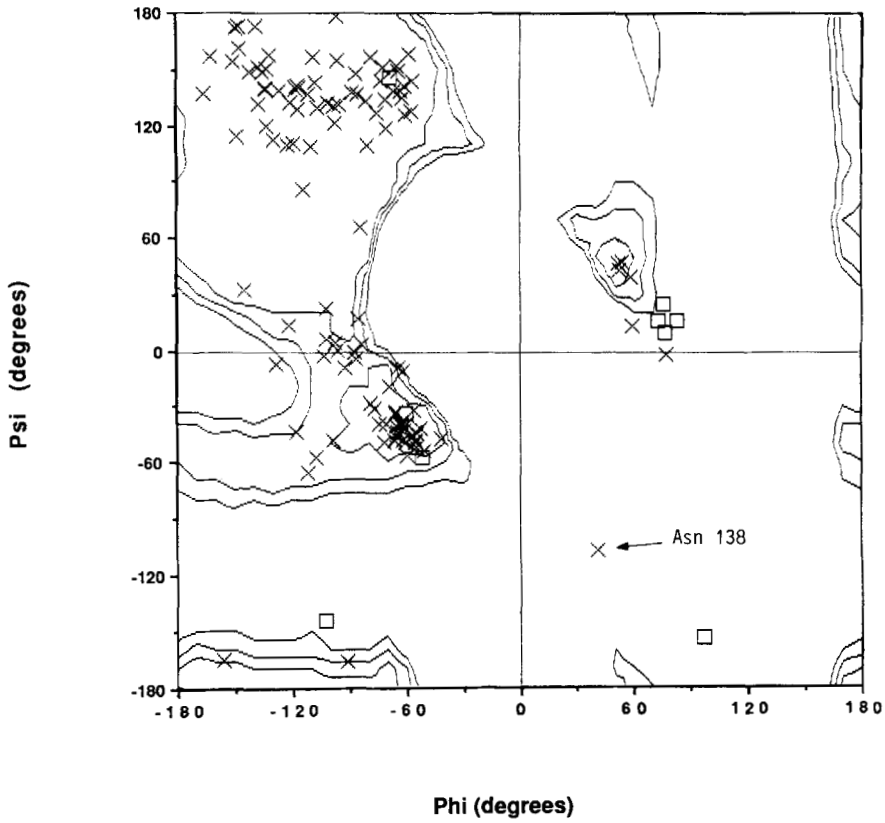

Fig. 7. Ramachandran diagram for the refined nuclease–Ca^{2+}–pdTp structure. Glycine residues are marked by boxes (□), while nonglycine residues are marked by X's. Note the unfavorable position of Asn-138. Superimposed upon this diagram are iso-energy contours for the alanine dipeptide (see ref. 39); the energy map is contoured at 4, 6, and 8 kcal/mol. Grid points for the alanine dipeptide map were kindly supplied by Dr. Steven Sheriff.

carboxyl interaction found to be prevalent by Singh et al.[33] The other terminal amino group of Arg-35 is hydrogen bonded to the backbone carbonyl oxygens of residues 36 and 39, and seems to hold this arginine poised in the optimal position for binding the inhibitor's (and presumably the substrate's) 5′-phosphate. Two of the oxygens of the 5′-phosphate, including the ester oxygen, are hydrogen bonded to the two terminal amines of Arg-87. Just as Arg-35 is held in position where it may interact with the inhibitor, so Arg-87 is tethered by a hydrogen bond to the side chain of Asp-83 (in the nomenclature of Singh et al., this is a type 9 interaction). In addition to the bonds formed with Arg-35 and Arg-87, an oxygen from the 5′-phosphate is involved in a ionic interaction with the Ca^{2+}, and there are four waters

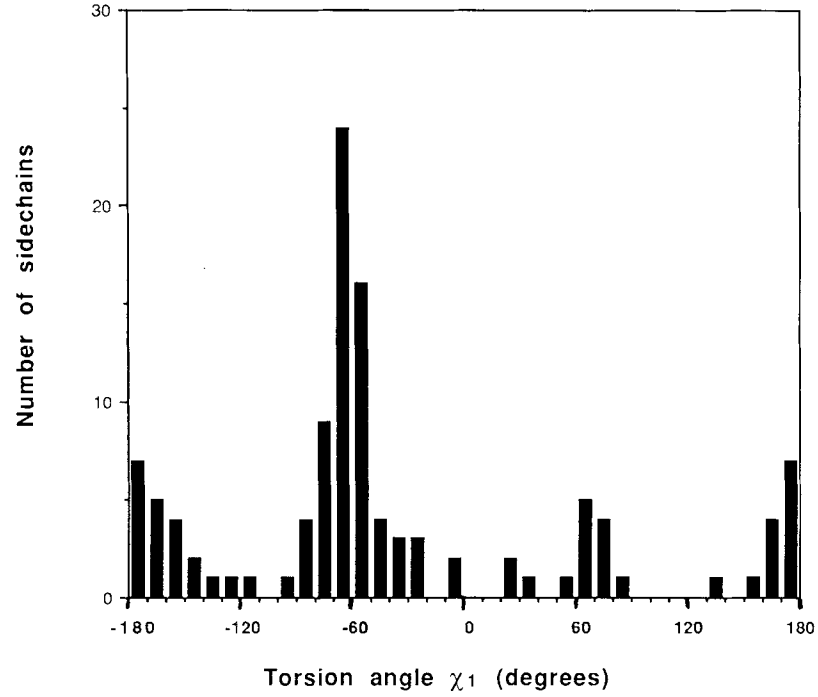

Fig. 8. Distribution of side chain torsion angles χ^1.

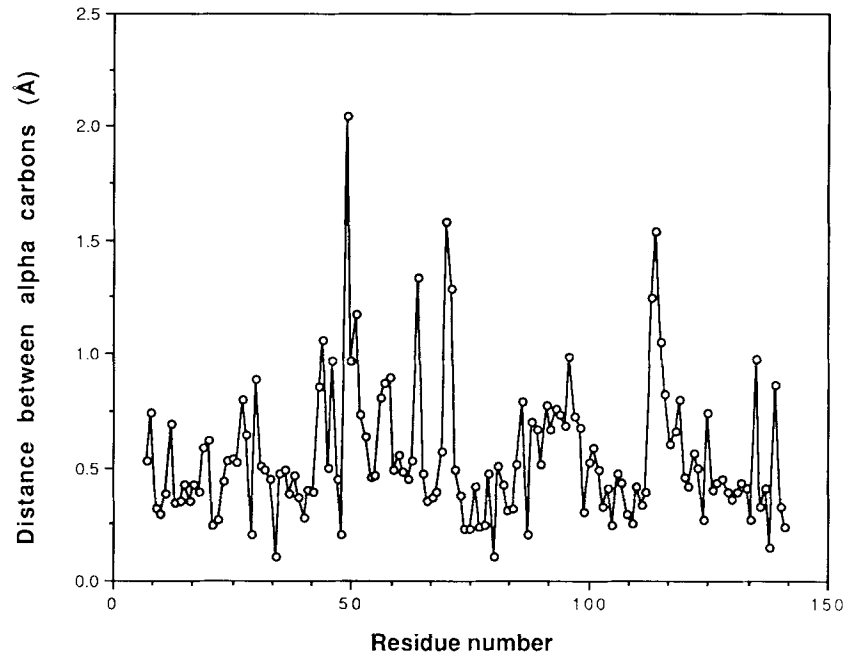

Fig. 9. Distance between corresponding C_α positions in refined and unrefined structures. The unrefined structure was superimposed upon the refined structure by a least-squares superposition technique which minimized C_α–C_α distances; residues in the mobile loop between residues 45 and 50 were omitted from the calculation to obtain the best fit. The motions required to superimpose the two molecules turned out to be negligible, i.e., the orientation and position of the molecule in the unit cell have not changed with refinement.

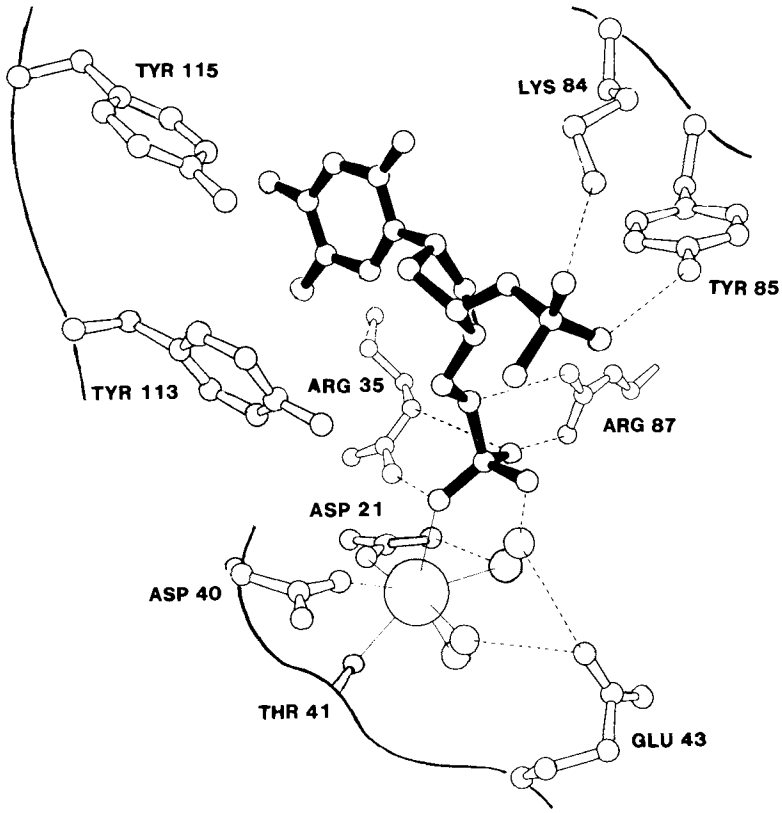

Fig. 10. Schematic drawing of the active site. Protein side chains are shown by light bonds, while the pdTp molecule is in dark. The calcium ion is shown as the large sphere below the inhibitor molecule. Also shown are the three inner sphere water ligands of the calcium ion and the water molecule bridging Glu-43 and the 5′-phosphate of the inhibitor (this bridging water is the putative nucleophile in the hydrolysis of phosphoesters).

hydrogen bonded to 5′-phosphate oxygens. Thus, every potential hydrogen bond acceptor in the 5′-phosphate is involved in at least two hydrogen bonds except the ester oxygen, which accepts a single hydrogen bond from Arg-87; the 5′-phosphate is therefore tightly locked into place by a network of hydrogen bonds and ionic interactions which serve both to position it and neutralize its negative charge.

It is important to note that a possible artifact of crystallization may affect the interpretation of the active site structure. Lys-70* and Lys-71* from an adjacent molecule in the crystal lattice protrude into the active site (we use the * here to denote a residue from such an adjacent symmetry mate). The ϵ-amino of Lys-71* is positioned precisely halfway between the 3′- and 5′-phosphates of pdTp, and makes strong hydrogen bonds to oxygens on each group, and the ϵ-amino of Lys-70* takes part in a salt bridge with Glu-43. Now, as described above, the 5′-phosphate of the inhibitor is held tightly in position, even if one removes the hydrogen bond contributed by Lys-71*. On the other hand, the 3′-phosphate, while evidently firmly bound, is not so firmly bound as the 5′-phosphate, and it is possible to imagine that in the absence of the positive charge and hydrogen bonding contribution of Lys-71* the 3′-phosphate of the inhibitor would not occupy the same position as it does in our structure. However, moving the 3′-phosphate closer to the metal in order to mimic a structure proposed by Serpersu et al.[34,35] would entail pulling the pdTp ring partially out of its hydrophobic pocket and/or disrupting the very tight binding of the 5′-phosphate; it is difficult to envision a favorable way of accomplishing either of these movements. The only certain way to elucidate if lysines 70* and 71* are distorting the binding of pdTp in the active site is to determine the structure of a mutant nuclease in which these lysines have been altered, perhaps to alanines. We are exploring the possibility of determining such a mutant structure.

All of the interactions described thus far have already been noted by Cotton et al., or are consistent with their observations. The refined model differs from the unrefined model in the vicinity of the metal ion and the putative general base, Glu-43, but the differences do not affect the mechanistic conclusions drawn by the earlier workers. The coordination of

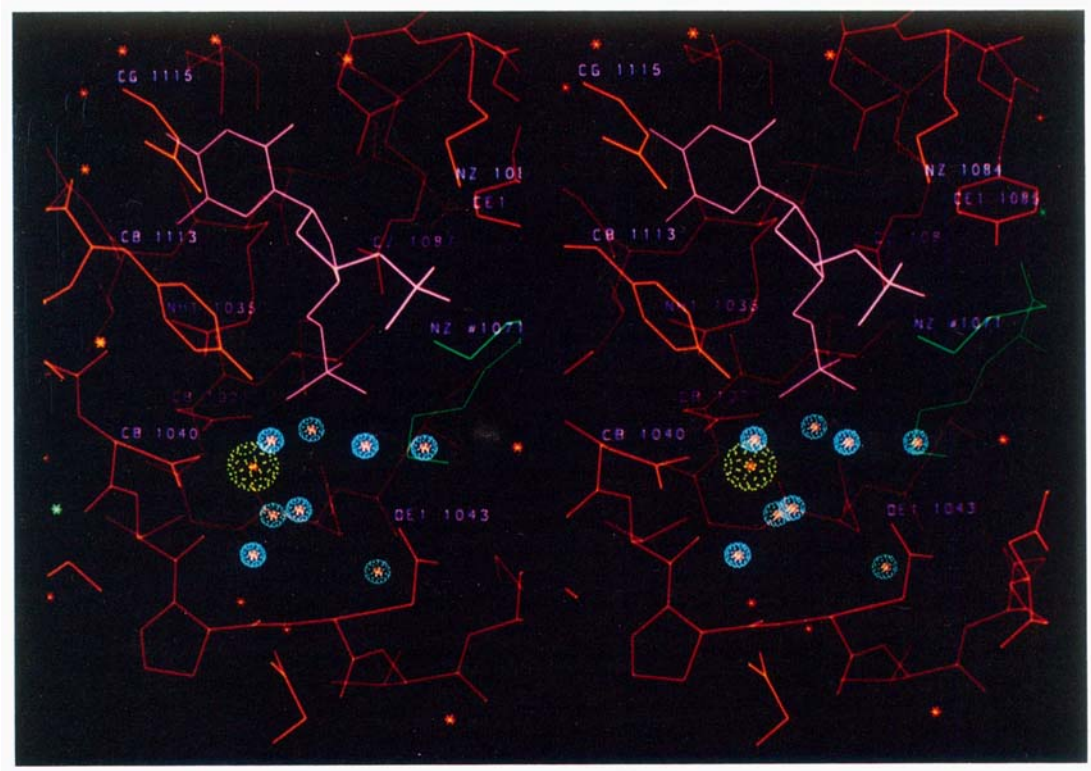

Fig. 11. Stereo view of an active site model generated in the program FRODO.[20] Protein atoms are shown in orange, while the pdTp molecule is light pink. The calcium ion is represented by a large stippled green ball, and water molecules actually in the active site are represented by smaller blue stippled balls. Note the presence of lysines 70* and 71* (shown here in green) on the right side of picture; these side chains are contributed by an adjacent protein molecule in the crystal lattice. Note also that the numbering of residues is the same as in Figure 3; thus residue 43 is shown as 1043, etc.

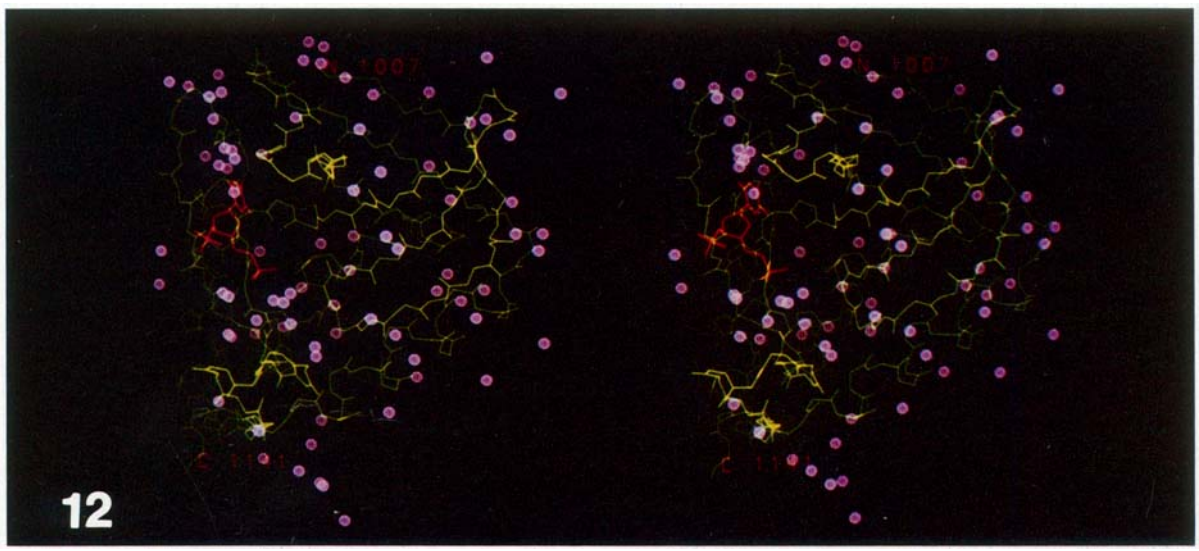

Fig. 12. Solvent water molecules found in the refined model. In this stereo view, the 82 water molecules are represented by lavender balls, shown in relation to the backbone of the protein. The pdTp molecule is also depicted (in orange). This view is taken from the same vantage point as Figure 6, with the N-terminus in the upper right and the C-terminus in the lower left.

the calcium ion can be described as octahedral, except that the position that would normally occupied by one of the polar ligands is shared by two oxygen atoms (a water molecule and the carbonyl oxygen of Thr-41), giving the metal seven ligands rather than six. Of these seven ligands, three are contributed by the protein, three are tightly bound solvent waters, and one is an oxygen on the 5′-phosphate of the inhibitor pdTp.

One of the calcium's water ligands is hydrogen bonded to the sidechain of Glu-43. Our model shows that this water ligand is adjacent to the ligand contributed by Asp-40, not opposite, as was shown in the earlier model. However, we do clearly see and confirm the existence of another water molecule which is not in the inner coordination sphere of the metal ion, but which is bridging the side chain of Glu-43 and the 5′-phosphate. This water was described by the earlier workers, and was proposed as a candidate for the attacking nucleophile during hydrolysis of the phosphate ester. Examination of the refined structure reveals that *both* water molecules hydrogen-bonded to the side chain of Glu-43 (the bridging water and the calcium ligand) are close enough to the 5′-phosphorus (3.7 and 4.4 Å, respectively) to be candidates for the attacking nucleophile.

The mechanism proposed for staphylococcal nuclease by Cotton et al.[9] postulates that Glu-43, acting as a general base, deprotonates the water bridging it to pdTp's 5′-phosphate; this water becomes the attacking nucleophile during the subsequent hydrolysis. Polarization of the phosphate is achieved by interactions with the Ca^{2+} ion and arginines 35 and 87, while Arg-87 protonates the leaving group. Our refined structure confirms all of the features which underlie this hypothesis, and is entirely consistent with the proposed mechanism. We offer four comments: (1) The proposed mechanism is predicated upon the assumption that the structure of the enzyme–Ca^{2+}–pdTp complex is a good model for the productive complex of enzyme, Ca^{2+}, and substrate. While evidence is cited in support of this assumption,[1–4] the assumption cannot be taken as proven; we are particularly concerned about any changes in the binding of the inhibitor which are caused by the proximity of the symmetry-related lysines 70* and 71*. (2) It is necessary to invoke a general acid to protonate the leaving group to explain the efficient cleavage of the phosphoester. On the basis of our structure (again, assuming that this inhibited structure provides a valid model for catalysis), we can state that the only candidate for the general acid is Arg-87. The phenolic hydroxyl of Tyr-113 does not hydrogen bond to the ester oxygen, nor can it be brought close to this oxygen by combinations of simple rotations of the side chain χ^1 and χ^2 angles; major backbone motions would need to be invoked. Further evidence that Tyr-113 does not act as a general acid in nucleic acid hydrolysis is given by the fact that the mutant nuclease Y113F (Tyr-113→Phe) displays wild-type activity (J. Gerlt, personal communication). No other protein group appears to be reasonable, and no appropriate solvent atoms are in evidence, so Arg-87 is the only likely side chain which can activate the substrate. Arginine sidechains typically have very high p*K*'s, and thus Arg-87 may seem like an unlikely general acid. However, if proton transfer takes place after formation of the transition state, and not beforehand, an arginine should be perfectly capable of acting as a proton donor (since the leaving group should be even more basic than the arginine). (3) Enzymatic studies have shown that nuclease requires two equivalents of Ca^{2+} for catalytic activity,[36] yet only one Ca^{2+} ion is present in the crystal structure. This is another reason why we cannot be certain that the structure we observe is a good model for the productive complex. (4) We cannot firmly state which of the water molecules (if any) seen in the refined structure corresponds to the attacking nucleophile. The water bridging Glu-43 and pdTp's 5′-phosphate, the candidate put forward by Cotton et al., is in an excellent position. The water bridging Glu-43 and the calcium ion, however, is still reasonably close to the phosphorus atom and cannot be ruled out.

Solvent Structure

Eighty-two water molecules have been located in the final structure; these waters, along with a trace of the α carbon backbone, are shown in Figure 12. We see no evidence in the maps for the presence of ordered MPD molecules or phosphate anions. Of the 82 waters, 33 have unit occupancies, and the remainder have occupancies ranging from 0.50 to 0.99. Examination of the distribution of distances from waters to their nearest protein atoms shows a sharp clustering centered at 2.85 Å, with small tails at both longer and shorter distances. It appears, then, that we are seeing bound waters only in the first shell of hydration. We observe no evidence for pentagonal clustering of water molecules.

The surface area of the protein which is accessible to solvent has been calculated by the method of Lee and Richards,[37] and is plotted as a function of residue number in Figure 13, along with the crystallographic temperature factors. The expected approximate correlation between the solvent accessibility of a residue and its mean temperature factor is observed. The mean temperature factor for all atoms in the model is 26.6 $Å^2$, which is in good agreement with the figure obtained from Wilson statistics (data not shown).

Crystal Packing

Each protein molecule contacts four neighboring molecules in the crystal lattice; three unique interfaces are involved in these contacts. The most exten-

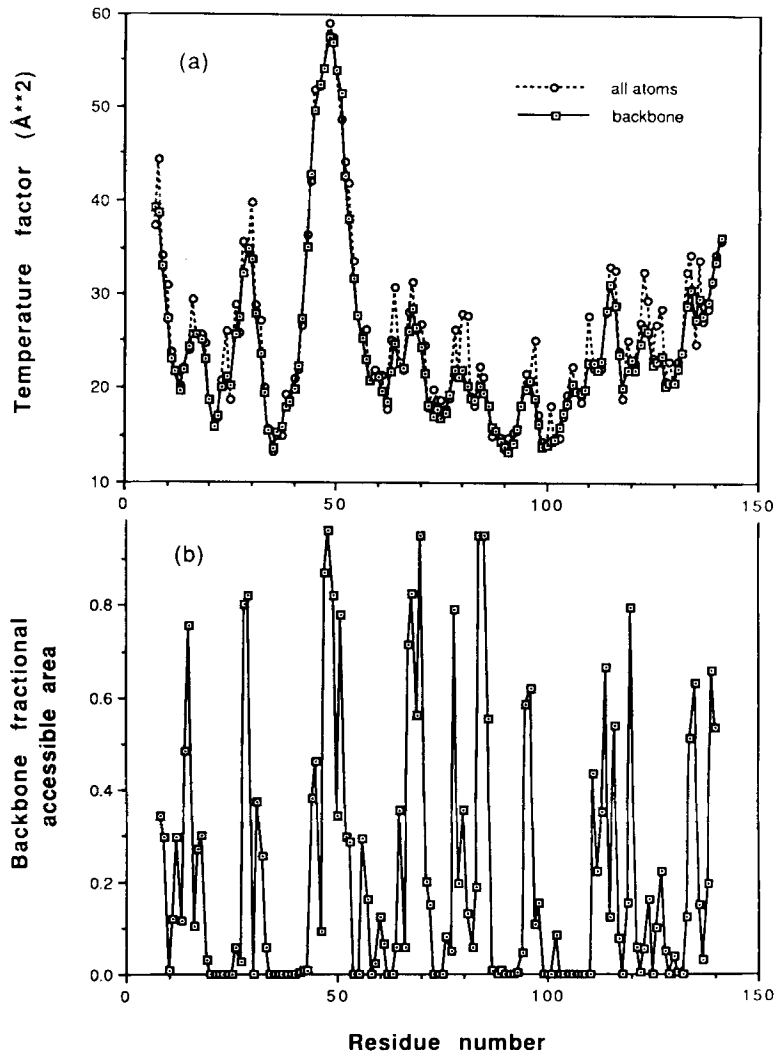

Fig. 13. **a:** Mean temperature factors for each residue in the refined model. The solid line represents the mean B-factor of the backbone atoms for each residue (N, C_α, carbonyl C, and carbonyl O), while the dotted line represents the mean B-factor for all atoms of each residue. **b:** Fractional solvent accessible area for each residue in the refined model. We employed the program ACCESS, written by M. Handschumacher and F. M. Richards, which implements the algorithm of Lee and Richards.[37] Solvent accessible area was calculated for the backbone atoms of each residue; fractional accessible areas were then calculated as the ratios of the observed accessible areas to the accessible areas of the same residues in Ala-X-Ala tripeptides.

sive interface packs the bend region around residue 80 against the C-terminal end of a neighboring molecule. If one examines a protein molecule and the two neighbors which are related to it by this contact, one sees that the three molecules are lined up almost precisely along the crystal's *c* axis. The other two interfaces place (1) the start of the first β strand (around residue 12) against the bend at residues 84–85 of a neighbor, and (2) the bend at lysines 70 and 71 into the active site cleft of the same neighboring molecule. In contrast to the first interface, these two interfaces represent contacts which lie almost exclusively in the *a–b* plane of the crystal. It is noteworthy that our calculated values of the anisotropic ΔB tensor seem to indicate that motion (or disorder) in the molecule's *x–y* plane (the *a–b* plane of the crystal) is more extensive than motion (disorder) along the molecule's *z* axis (the crystalline *c* axis); i.e., b_{11} and b_{22} are positive, whereas b_{33} is negative. This is consistent with a simple model in which the large contact areas along the molecular *z* axis damp motion along the crystalline *c* axis, while the smaller contact areas in the *x–y* plane allow freer motion in the crystal *a–b* plane. Analysis of mutant forms of nuclease which crystallize in space groups other than $P4_1$,[38] which presumably possess a different set of intermolecular contacts, will enable us to explore this further.

We intend to deposit both our structure factors and the coordinates of our model in the Brook-

APPENDIX: INTRAMOLECULAR HYDROGEN BONDS

TABLE AI. Helical Hydrogen Bonds

Donor* (D)	Acceptor* (A)	D–A distance (Å)	D . . . A-carbon angle (°)
A58N	Y54O	2.78	159
S59N	G55O	3.05	156
A60N	P56O	3.05	145
F61N	E57O	2.91	155
T62N	A58O	3.14	152
K63N	S59O	2.93	150
K64N	A60O	2.92	152
M65N	F61O	2.97	163
V66N	T62O	2.88	165
E67N	K63O	2.68	164
N68N	K64O	2.93	155
A102N	M98O	3.01	159
L103N	V99O	3.10	154
R105N	E101O	2.75	167
Q106N	A102O	3.19	150
L125N	H121O	2.91	161
R126N	E122O	2.69	148
K127N	Q123O	2.79	158
S128N	H124O	3.14	157
E129N	L125O	3.03	156
A130N	R126O	3.15	154
Q131N	K127O	3.27	156
A132N	S128O	3.05	153
K133N	E129O	2.91	149
K134N	A130O	2.74	151
E135N	Q131O	2.81	156
K136N	A132O	3.10	139
Mean		2.96 ± 0.16	155 ± 6

*Identifiers for donor and acceptor atoms: single letter amino acid code, residue number, and atom name.

TABLE AII. β Sheet Hydrogen Bonds

Donor* (D)	Acceptor* (A)	D–A distance (Å)	D . . . A-carbon angle (°)
I18N	T22O	3.05	140
D19N	T22O	3.08	151
L36N	D21O	2.91	163
L37N	A90O	2.86	138
E10N	V74O	2.86	158
V74N	E10O	2.79	165
A12N	I72O	3.18	134
T13N	M26O	2.91	145
M26N	T13O	2.78	157
I15N	K24O	2.90	138
K16N	K24O	3.12	131
K24N	K16O	2.72	157
V23N	F34O	3.05	157
F34N	V23O	2.79	161
L25N	M32O	2.73	170
M32N	L25O	2.80	171
Y27N	Q30O	2.80	135
Q30N	Y27O	2.92	114
G88N	T33O	2.70	151
R35N	G88O	2.66	178
E73N	Y93O	2.88	149
Y93N	E73O	2.64	157
D95N	K71O	2.94	164
E75N	Y91O	2.68	158
Y91N	E75O	2.81	147
Mean		2.86 ± 0.15	152 ± 15

*Identifiers for donor and acceptor atoms: single letter amino acid code, residue number, and atom name.

TABLE AIII. Other Main Chain to Main Chain Hydrogen Bonds

Donor* (D)	Acceptor* (A)	D–A distance (Å)	D . . . A-carbon angle (°)
A112N	L38O	3.09	112
D40N	K110O	3.08	166
K110N	D40O	3.12	141
E52N	E43O	2.92	155
K49N	H46O	3.02	111
G50N	H46O	2.58	157
G55N	E52O	3.06	129
L89N	R81O	2.87	129
G86N	D83O	2.82	125
D83N	R87O	2.98	155
V99N	I92O	2.75	164
A94N	K97O	2.76	144
K97N	A94O	2.91	115
L108N	L103O	2.77	162
G107N	V104O	2.90	121
I139N	G107O	3.01	151
N118N	Y115O	2.51	141
N119N	P117O	2.92	89
E122N	N119O	3.06	121
L137N	A132O	3.03	166
K136N	L133O	2.92	110
W140N	L137O	2.77	129
S141N	N138O	2.44	134
Main		2.88 ± 0.19	136 ± 21

*Identifiers for donor and acceptor atoms: single letter amino acid code, residue number, and atom name.

TABLE AIV. Main Chain to Side Chain Hydrogen Bonds

Donor* (D)	Acceptor* (A)	D–A distance (Å)	D . . . A-carbon angle (°)
K48N	H46ND1	2.44	
T22N	D19OD2	3.16	158
T41N	D21OD1	2.99	127
K45N	E43OE2	2.68	129
H46N	E43OE2	2.83	98
E43N	E52OE2	2.63	152
K70N	D95OD1	2.74	106
K71N	D95OD2	2.90	128
K78N	D77OD1	2.83	97
N119N	D77OD2	3.19	114
T120N	D77OD2	2.90	124
G79N	N118OD1	2.69	151
Y85N	D83OD1	2.94	121
G86N	D83OD1	3.21	166
R87N	D83OD1	2.99	139
H121N	Y91OH	3.29	110
I92N	N100OD1	3.12	139
V111N	E129OE1	2.64	130
R35NH1	L36O	2.72	146
R35NH1	V39O	2.76	141
R35NH2	V39O	3.08	139
N100ND2	L37O	2.86	126
K110NZ	D40O	3.03	128
N118ND2	Q80O	3.01	136
N138ND2	Q106O	2.48	173
T62OG1	G20O	2.54	123
T62OG1	A58O	3.16	154
S141OG	N138O	2.55	131
Mean		2.87 ± 0.24	128 ± 31

*Identifiers for donor and acceptor atoms: single letter amino acid code, residue number, and atom name.

TABLE AV. Side Chain to Side Chain Hydrogen Bonds

Donor* (D)	Acceptor* (A)	D–A distance (Å)	D . . . A-carbon angle (°)
K9NZ	E75OE1	3.27	131
R35NH2	D40OD1	3.28	115
H121NE2	E75OE2	2.94	128
K78NZ	T120OG1	2.91	132
R87NE	D83OD2	2.84	128
R87NH2	D83OD2	2.83	163
K84NZ	Y85OH	3.28	98
R105NH1	E135OE1	3.00	100
R105NH2	E135OE1	3.26	85
R105NH2	E135OE2	2.85	104
N119ND2	E122OE2	3.22	159
R126NE	E122OE1	2.58	113
R126NH2	E122OE1	2.97	141
Q131NE2	E135OE2	2.74	125
Y27OH	E10OE1	2.83	109
T22OG1	D21OD2	3.08	149
Y54OH	S141OG	3.26	157
Y93OH	E75OE2	2.60	121
Y91OH	D77OD2	2.56	149
T120OG1	D77OD1	2.44	125
S128OG	E101OE1	2.43	116
Mean		2.91 ± 0.28	126 ± 21

*Identifiers for donor and acceptor atoms: single letter amino acid code, residue number, and atom name.

haven Protein Data Bank upon acceptance of this report.

ACKNOWLEDGMENTS

We thank David Shortle for supplying overproducing strains of *E. coli*, as well as for advice and encouragement, and Charles Carter and his colleagues at the University of North Carolina for their hospitality and assistance. This work was funded by Grant GM-36358-03 from the National Institutes of Health.

REFERENCES

1. Tucker, P. W., Hazen, E. E., Jr., Cotton, F. A. Staphylococcal nuclease reviewed: A prototypic study in contemporary enzymology. I. Isolation; physical and enzymatic properties. Mol. Cell. Biochem. 22:67–77, 1978.
2. Tucker, P. W., Hazen, E. E., Jr., Cotton, F. A. Staphylococcal nuclease reviewed: A prototypic study in contemporary enzymology. II. Solution studies of the nucleotide binding site and the effects of nucleotide binding. Mol. Cell. Biochem. 23:3–17, 1979.
3. Tucker, P. W., Hazen, E. E., Jr., Cotton, F. A. Staphylococcal nuclease reviewed: A prototypic study in contemporary enzymology. III. Correlation of the three-dimensional structure with the mechanisms of enzymatic action. Mol. Cell. Biochem. 23:67–86, 1979.
4. Tucker, P. W., Hazen, E. E., Jr., Cotton, F. A. Staphylococcal nuclease reviewed: A prototypic study in contemporary enzymology. IV. The nuclease as a model for protein folding. Mol. Cell. Biochem. 23:131–141, 1979.
5. Shortle, D. A genetic system for analysis of staphylococcal nuclease. Gene 22:181–189, 1983.
6. Shortle, D., Lin, B. Genetic analysis of staphylococcal nuclease: Identification of three intragenic "global" suppressors of nuclease-minus mutants. Genetics 110:539–555, 1985.
7. Takahara, M., Hibler, D. W., Barr, P. J., Gerlt, J. A., Inouye, M. The *ompA* signal peptide directed secretion of staphylococcal nuclease A by *E. coli*. J. Biol. Chem. 260: 2670–2674, 1985.
8. Hibler, D. W., Stolowich, N. J., Reynolds, M. A., Gerlt, J. A., Wilde, J. A., Bolton, P. H. Site-directed mutants of staphylococcal nuclease. Detection and localization by ^1H NMR spectroscopy of conformational changes accompanying substitutions for glutamic acid 43. Biochemistry 26: 6278–6286, 1987.
9. Cotton, F. A., Hazen, E. E., Jr., Legg, M. J. Staphylococcal nuclease: Proposed mechanism of action based on structure of enzyme-thymidine 3′,5′-bisphosphate-calcium ion complex at 1.5 Å resolution. Proc. Natl. Acad. Sci. U.S.A. 76:2551–2555, 1979.
10. Serpersu, E. H., Shortle, D., Mildvan, A. S. Kinetic and magnetic resonance studies of effects of genetic substitution of a Ca^{2+}-liganding amino acid in staphylococcal nuclease. Biochemistry 25:68–77, 1986.
11. Cotton, F. A., Hazen, E. E., Jr., Richardson, D. C. Crystalline extracellular nuclease of *Staphylococcus aureus*. J. Biol. Chem. 241:4389–4390, 1966.
12. Arnone, A., Bier, C. J., Cotton, F. A., Hazen, E. E., Jr., Richardson, D. C., Richardson, J. S. The extracellular nuclease of *Staphylococcus aureus:* Structures of the native enzyme and an enzyme-inhibitor complex at 4 Å resolution. Proc. Natl. Acad. Sci. U.S.A. 64:420–427, 1969.
13. McPherson, A. "Preparation and Analysis of Protein Crystals." New York: J. Wiley, 1982: 96–97.
14. Hendrickson, W. A. Stereochemically restrained refinement of macromolecular structures. In: Diffraction Methods for Biological Macromolecules, "Methods in Enzymology," Vol. 115. New York: Academic Press, 1985: 252–270.
15. Sheriff, S. Addition of symmetry-related contact restraints to PROTIN and PROLSQ. J. Appl. Crystallogr. 20:55–57, 1987.
16. Smith J. L., Hendrickson, W. A., Honzatko, R. B., Sheriff, S. Structural heterogeneity in protein crystals. Biochemistry 25:5018–5027, 1986.
17. Bernstein, F. C., Koetzle, T. F., Williams, G. J. B., Meyer, E. F., Jr., Brice, M. D., Rodgers, J. R., Kennard, O., Shimanouchi, T., Tasumi, M. The Protein Data Bank: A computer-based archival file for macromolecular structures. J. Mol. Biol. 112:535–542, 1977.
18. Abola, E. E., Bernstein, F. C., Bryant, S. H., Koetzle, T. F., Weng, J. In: "Crystallographic Databases—Information

Content, Software Systems, Scientific Applications." F. H. Allen, G. Bergerhoff, and R. Sievers, eds. Bonn/Cambridge/Chester: Data Commission of the International Union of Crystallography. 1987: 107–132.
19. Drew, H. R., Wing, R. M., Rakano, T., Broka, C., Tanaka, S., Itakura K., Dickerson, R. E. Structure of a B-DNA dodecamer: Conformation and dynamics. Proc. Natl. Acad. Sci. U.S.A. 78:2179–2183, 1981.
20. Jones, T. A. In: "Computational Crystallography." D. Sayre, ed., New York: Oxford University Press, 1982: 303–317.
21. Steigemann, W. "Die Entwicklung und Anwendung von Rechenverfahren und Rechenprogrammen zur Strukturanalyse von Proteinen am Beispiel des Trypsin-Trypsininhibitor Komplexes, des freien Inhibitors und der L-Asparaginase." Ph.D. thesis, Technical University Munich, 1974.
22. Sheriff, S., Hendrickson, W. A. Description of overall anisotropy in diffraction from macromolecular crystals. Acta Crystallogr. A43:118–121, 1987.
23. Cruickshank, D. W. J. The accuracy of electron-density maps in x-ray analysis with special reference to dibenzyl. Acta Crystallogr. 2:65–82, 1949.
24. Cruickshank, D. W. J. The accuracy of electron density maps in x-ray analysis: correction. Acta Crystallogr. 7:519, 1954.
25. Cruickshank, D. W. J. Fourier synthesis and structure factors. In: "International Tables for X-Ray Crystallography." J. S. Kasper and K. Lonsdale, eds. Birmingham, England: Kynoch Press, 1959: 317–338.
26. Luzatti, P. V. Traitement statistique des erreurs dans la determination des structures cristallines. Acta Crystallogr. 5:802–810, 1952.
27. Chambers, J. L., Stroud, R. M. The accuracy of refined protein structures: Comparison of two independently refined models of bovine trypsin. Acta Crystallogr. B35:1861–1874, 1979.
28. Richardson, J. S. The anatomy and taxonomy of protein structure. Adv. Protein Chem. 34:167–339, 1981.
29. Schellman, C. The α_L conformation at the ends of helices. In: "Protein Folding." R. Jaenicke, ed. New York: Elsevier/North-Holland Biomedical Press, 1980: 53–61.
30. Presta, L. G., Rose, G. D. Helix signals in proteins. Science 240:1632–1641, 1988.
31. Janin, J., Wodak, S., Levitt, M., Maigret, B. Conformation of amino acid side-chains in proteins. J. Mol. Biol. 125:357–386, 1978.
32. Bhat, T. N., Cohen, G. H. OMITMAP: An electron density map suitable for examination of errors in a macromolecular model. J. Appl. Crystallogr. 17:244–248, 1984.
33. Singh, J., Thornton, J. M., Snarey, M., Campbell, S. F. The geometries of interacting arginine-carboxyls in proteins. FEBS Lett. 224:161–171, 1987.
34. Serpersu, E. H., McCracken, J., Peisach, J., Mildvan, A. S. Electron spin echo modulation and nuclear relaxation studies of staphylococcal nuclease and its metal coordination mutants. Biochemistry 27:8034–8044, 1988.
35. Serpersu, E. H., Hibler, D. W., Gerlt, J. A., Mildvan, A. S. Kinetic and magnetic resonance studies of the Glu-43 to Ser mutant of staphylococcal nuclease. Biochemistry 28: 1539–1548, 1989.
36. Cuatrecasas, P., Fuchs, S., Anfinsen, C. B. The binding of nucleotides and calcium to the extracellular nuclease of *Staphylococcus aureus*. J. Biol. Chem. 242:3063–3067, 1967.
37. Lee, B., Richards, F. M. The interpretation of protein structures: Estimation of static accessibility. J. Mol. Biol. 55:379–400, 1971.
38. Loll, P. J., Meeker, A. K., Shortle, D., Pease, M., Lattman, E. E. Crystallization and preliminary x-ray analysis of a quadruple mutant of staphylococcal nuclease. J. Biol. Chem. 263:18190–18192, 1988.
39. Peters, D., Peters, J. Quantum theory of the structure and bonding in proteins—Part 8: The alanine dipeptide. J. Mol. Structure 85:107–123, 1981.